Part I: Spatial Sensitivity and Intensity Distributions

Chapter 2

Characterization of fiber distributed-feedback lasers with an index perturbation method[1]

Abstract — We demonstrate characterization of fiber distributed-feedback lasers by scanning a heat-induced index perturbation along the cavity and by measuring the induced laser frequency shift. The measured shift is shown to be a good indicator for the intensity distribution in the cavity, and the experimental results reveal that the sensitivity of fiber distributed-feedback laser sensors with frequency read-out is highly localized near the grating phase-shift position. Use of the characterization data to determine the grating coupling parameter κ, the polarization dependence of κ, and birefringence non-uniformities as well as identification of the order of longitudinal mode operation are discussed and demonstrated experimentally. Asymmetrically phase-shifted lasers with highly directional output are also investigated.

OCIS codes: 140.3430, 140.3510, 140.4780, 230.1480, 050.2770, 060.2370.

2.1 Introduction

The modal intensity distribution within distributed-feedback (DFB) lasers depends distinctly on the order of longitudinal-mode operation, as well as grating properties such as the grating amplitude and phase. Measurements of modal intensity distributions can therefore be an attractive tool for the characterization of such devices.

[1]This chapter is a re-edited version of [E. Rønnekleiv, M. Ibsen, M. N. Zervas, and R. I. Laming, "Characterization of fiber distributed-feedback lasers with an index perturbation method", Appl. Opt., Vol. 38, pp. 4558-4565, 1999].

Few experiments have been reported on spatially resolved measurements of the lasing conditions within DFB-cavities, and the understanding of the modal field distributions depends to a high extent on theoretical models that are based on idealized assumptions. Spatially resolved measurements of spontaneous side-emission from semiconductor DFB lasers have been demonstrated [1, 2]. These measurements confirm the existence of spatial gain hole burning, and that different modes have different spatial intensity distributions. However, little quantitative information on the properties of the devices could be deduced from these measurements.

Deduction of the intensity distribution along an Er^{3+} fiber DFB laser from measurements of the green side-emission generated from excited-state absorption of the 980-nm pump signal has been demonstrated [3]. This method relies on a good knowledge of the energy transitions involved in the fiber, and it seems to be restricted to laser operation close to threshold. The method cannot be used with other pumping schemes or gain media.

A heat-scan technique for characterization of a fiber grating device was first demonstrated by Margulis *et.al.* in [4]. They scanned a heating wire along a fiber used for optical second harmonic (SH) generation. By monitoring the SH generation efficiency versus heating position they were able to determine the spatial distribution of the amplitude of a Bragg grating which assisted the SH generation in the fiber. Characterization of the spatial distribution of the Bragg wavelength in a chirped fiber Bragg grating with a heat-scan technique has later been demonstrated in [5]. [2]

Spatially resolved measurement of the grating phase and amplitude in a high reflectivity passive fiber Bragg grating was recently demonstrated [6]. The measurements were made by scanning a small heat-induced index perturbation along the grating and recording of the change in transmission at a wavelength outside the grating stopband.

From microwave theory it is known that one can measure the intensity distribution in a resonant cavity by moving a small refractive-index perturbation along the cavity and measuring the resulting shift in resonance frequency [7, 8]. In this paper we apply this principle, to our knowledge for the first time, to characterize optical fiber DFB resonators. Parts of the experiments reported in this paper have earlier been presented in a conference paper [9].

[2] The references to [5] and [4] were not included in the Applied Optics version of this manuscript. We apologize for this omission.

2.2 Theory

2.2.1 Modal Intensity Distributions and Gain Thresholds

When interference between the forward- and backward-propagating field amplitudes E_+ and E_-, respectively, is taken into account, the local intensity inside an optical cavity can be expressed as:

$$|E_{loc}(z)|^2 = |E_0|^2 + 2|E_+E_-|\cos(2\pi z n\nu/c + \theta), \tag{2.1}$$

where ν is the resonating optical frequency, n is the refractive-index of the fiber, c is the speed of light in vacuum, $|E_0|^2 = |E_+|^2 + |E_-|^2$ is the mean intensity, $2|E_+E_-|$ is the standing wave intensity modulation amplitude, and θ is the standing wave modulation phase. $|E_0|^2$, $|E_+|^2$, $|E_-|^2$ and θ may all be slowly varying functions of z.

Figure 2.1 shows the theoretical intensity distributions of the fundamental mode and the first and second higher order mode pairs in a $L = 60$ mm index-coupled DFB structure, obtained by a T-matrix approach [15, 16, 17, 18].[3] The illustrated grating has a coupling coefficient of $\kappa = 230$ m^{-1} and a π grating phase-shift at the center. A uniform gain of 4.1×10^{-3} dB/m is required for lasing in the fundamental mode, whereas 22.0 dB/m and 31.5 dB/m are required for the first and second higher order mode pairs, respectively. The fundamental mode in this case is the mode operating at the Bragg resonance frequency ν_{Bragg}. For the illustrated κL-product of 13.8, the first and second higher-order mode pairs are found to operate at $\nu_{\pm 1} = \nu_{Bragg} \pm 1.086 v_g\kappa/(2\pi)$ and $\nu_{\pm 2} = \nu_{Bragg} \pm 1.111 v_g\kappa/(2\pi)$, respectively, i.e., close to the stopband edges of the uniform grating, defined as $\nu_{Bragg} \pm v_g\kappa/(2\pi)$.[4] Here v_g is the group velocity of the uncoupled waveguide.

In the more general case, one may consider an asymmetrically phase-shifted DFB laser of length L with the phase-shift positioned at $z = -\Delta L/2$ relative to the grating center $z = 0$. For such a laser the following approximations are valid, provided that the left and right sub-gratings are both relatively strong, i.e. $\kappa|L - \Delta L| \gtrsim 1$:

$$|E_0|^2 \approx P_0 \frac{\cosh\kappa(L \pm 2z)}{\cosh\kappa(L \mp \Delta L)}, \tag{2.2}$$

$$2|E_+E_-| \approx P_0 \frac{\sinh\kappa(L \pm 2z)}{\cosh\kappa(L \mp \Delta L)}, \tag{2.3}$$

[3] A more detailed description of the T-matrix DFB laser model is given in Chap. 6, which is a re-edited version of [18].

In the Applied Optics version of the present chapter, a wrong reference number was used for [18]. We have here also added references to some early papers [15, 16, 11] where T-matrixes for optical Bragg grating and DFB laser modelling are introduced.

[4] In the original paper, the factor $1/(2\pi)$ is missing in the expressions for the mode frequency spacing and the stop-band width. The expressions given here are correct.

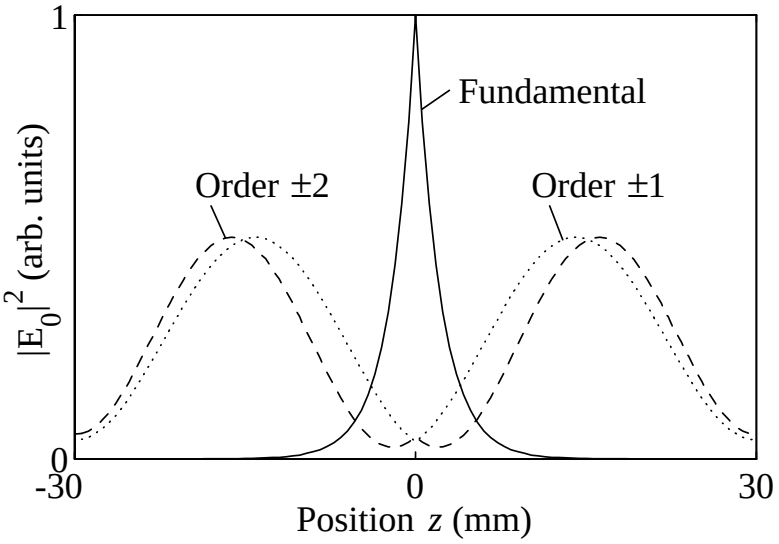

Figure 2.1. Theoretical intensity distribution $|E_0|^2$ in a 60 mm laser with $\kappa = 230\text{m}^{-1}$ for the fundamental and first and second higher order modes.

where the upper signs apply for $-L/2 < z < -\Delta L/2$. P_0 is the intensity $|E_0|^2$ at $z = -\Delta L/2$.

Figure 2.2 shows the exact distributions of $|E_0|^2$, $2|E_+E_-|$, $|E_+|^2$, and $|E_-|^2$, calculated by the T-matrix approach, for an asymmetric laser with $\kappa L = 8$ and $\kappa\Delta L = 2$. As we explain in Subsection 2.2.2 below, the characterization method proposed in this paper produces a measure for the distribution of standing wave intensity amplitude $2|E_+E_-|$. From Fig. 2.2 and from expressions (2.2) and (2.3) one see that $|E_0|^2 \approx 2|E_+E_-| \approx \exp 2\kappa|z + \Delta L/2|$ at distances that are separated $\gtrsim \kappa^{-1}$ from the grating ends. This implies that the characterization method also produces a good estimate for the mean intensity distribution. It also implies that κ can be found easily from measurements of the exponential decay rate of $2|E_+E_-|$ or $|E_0|^2$ within the cavity.

The left to right output power ratio from the laser can be approximated from Eq. (2.2) as:

$$\frac{P_{left}}{P_{right}} = \frac{|E(-L/2)|^2}{|E(L/2)|^2} \approx \exp(2\kappa\Delta L) \tag{2.4}$$

An asymmetric π phase-shifted grating thus provides a simple way to make a laser with directional output power. This method was first demonstrated for fiber DFB lasers by movement of a thermally induced π phase-shift along a laser grating [10], yielding left to right output ratios of the order of 3–4.

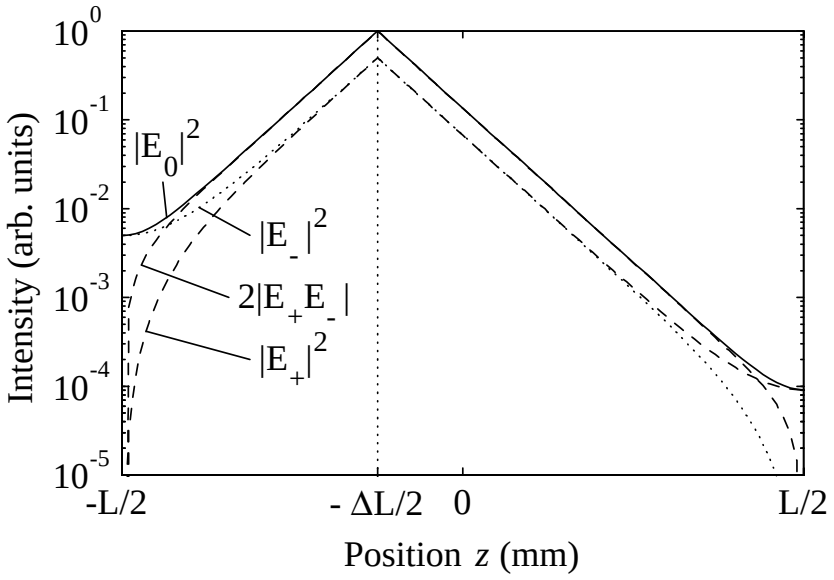

Figure 2.2. Theoretical distributions of $|E_+|^2$, $|E_-|^2$, $|E_+E_-|$ and $|E_0|^2 = |E_+|^2 + |E_-|^2$, calculated by the T-matrix approach, for an asymmetric laser with $\kappa L = 8$ and $\kappa \Delta L = 2$.

The method has also been discussed in a later publication [11]. The exact numerical calculations, assuming uniform gain distributions, show that Eq. (2.4) is a good approximation for grating parameters relevant for fiber lasers. For $\kappa(L - \Delta L) > 2$ and $P_{left}/P_{right} < 60$ dB the estimation error is within ± 0.01 dB. For semiconductor lasers, $\kappa(L - \Delta L) > 0.5$ and $P_{left}/P_{right} < 20$ dB are more realistic, resulting in estimation errors that are within ± 1.7 dB.

The intensity in the higher order modes may be interpreted as an interference between the two eigen-solutions of the coupled-mode equations. The difference in phase-propagation constants for these solutions result in sine-shaped intensity distributions at each side of the phase-shift discontinuity, as seen for the first and second order modes in Fig. 2.1. The number of peaks and troughs in the intensity distribution increases with the modal order.

For all modes the gain thresholds decrease with increasing κL. Our calculations show that grating phase imperfections generally reduces the threshold further for some of the higher order modes, while the fundamental mode threshold increases. Nonlinear index changes, which may for instance be due to self heating in the cavity, or to gain-dependent index changes, will contribute to such grating phase errors. Spatial gain hole-burning in combination with non-linear refractive-index changes may therefore lead to multiple-longitudinal-mode operation in high κL gratings, as discussed in other publications [1, 12].

In semiconductor lasers the gain differences that are due to hole-burning can be great, and multi-mode operation has been observed for grating strengths well below $\kappa L = 2.5$ [1, 2, 12].

Few studies have been made of the robustness of single longitudinal-mode operation in fiber DFB-lasers. Since the available single-pass gain in these lasers is relatively low, κL-products in the range from 5 to 10 are typically required to obtain threshold for the fundamental mode. For many applications it may be desirable to increase κL further. First, the sensitivity to external back reflections is expected to decrease with increasing κL [13]. Second, the Schawlow-Townes noise limit, which is believed to determine the laser phase noise at high frequencies [14], decreases with increasing κ and increasing L. Third, dual polarization lasers, which are interesting for polarimetric sensor applications, have been shown theoretically to be more robustly dual polarization for high κL-values [18]. In Subsection 2.3.4 of this paper we report on a DFB-laser with κ and L similar to the one modelled in Fig. 2.1 that was found to operate in a higher order mode. It is believed that the characterization method presented in this paper can be a useful tool for further investigations of longitudinal-mode competition in fiber DFB lasers.

2.2.2 Index-Perturbation Method

The index perturbation theory for resonant electromagnetic cavities [7, 8] states that a perturbation δn of the refractive-index within a small region δz of a cavity will result in a small shift $\delta\nu$ of the resonance frequency ν, given by:

$$\frac{\delta\nu}{\nu} = -\frac{\delta n \delta z \, |E_{loc}(z)|^2}{\int\limits_{Cavity} n(\hat{z}) \, |E_{loc}(\hat{z})|^2 \, d\hat{z}}. \tag{2.5}$$

Here z is the position of the perturbation and $|E_{loc}(\hat{z})|^2$ is the local intensity at position $\hat{z}$; *c.f.* Eq. (2.1). Equation (2.5) shows that $\delta\nu$ is proportional to the intensity at the perturbation point and to the induced round-trip phase perturbation $\delta\phi = 4\pi \, \delta n \delta z \, \nu/c$.

Both Cunliffe and Mathias [7] and Casimir [8] have deduced Eq. (2.5) (in slightly different 3-dimensional forms) for a gainless and lossless cavity medium with discrete and perfectly reflecting boundaries. This corresponds to zero net transport of energy within the cavity, implying that $|E_+|^2 = |E_-|^2$ everywhere. When the perturbed region is much larger than one standing wave period ($\delta z \gg nc/\nu$), $|E_{loc}|^2$ may therefore be replaced by $2|E_+E_-| = |E_+|^2 + |E_-|^2 = |E_0|^2$ in their treatment.

In a laser, there will always be transport of energy towards the output ports, i.e. $|E_+|^2 \neq |E_-|^2$. We have made exact numerical calculations of the perturbation sensitivity of the fundamental mode in π phase-shifted DFB lasers with

varying κL-products. A T-matrix approach, which is valid for $\delta z \gg nc/\nu$, was used for the calculations. The results show an exact agreement with Eq. (2.5), provided that $2|E_+E_-|$ is substituted for $|E_{loc}|^2$ in Eq. (2.5). An intuitive way of understanding this result, is by observing that $2|E_+E_-|$ constitutes the non-propagating (or recirculating) portion of the cavity intensity, being independent on power transport to the output ports.

Only perturbations of the cavity volume at the boundary is discussed in the paper by Cunliffe and Mathias [7]. An interesting discussion of the case with almost degenerate modes is however included. Casimir [8] generalizes the derivation to also include perturbations of the refractive-index within the cavity.

We have investigated the validity of Eq. (2.5) for DFB lasers numerically by the T-matrix approach. Based on the conditions stated by Cunliffe and Mathias [7] and Casimir [8], the following limitations have been identified:

1. The perturbation magnitude should be small. In practice this means that the round-trip phase perturbation $\delta\phi$ should be well below 1 rad, and that $\delta\nu$ should be much smaller than the spacing to other cavity modes.

2. The perturbation must not, to the first order in $\delta\phi$, introduce coupling between laser modes. That is, the perturbation of the global field distribution must be small to the first order in $\delta\phi$. This will generally be true if the mode investigated is not close to degeneration with other modes.

The last condition is generally not well satisfied for the DFB modes. However, as mentioned above, the numerically calculated response for the fundamental mode of ideal DFB lasers are found to be in exact agreement with Eq. (2.5), independent on κL, when substituting $|2E_+E_-|$ for $|E_{loc}|^2$. This result is believed to be related to the symmetry of the higher order modes relative to the fundamental mode. That is: any frequency shift due to coupling to the $+1$ mode is exactly compensated by coupling to the -1 mode, etc. The perturbation responses for the first and second higher order modes have been calculated for κL-values ranging from 1 to 18, yielding deviations from Eq. (2.5) (with $|2E_+E_-|$ substituted for $|E_{loc}|^2$) that are maximum $\pm 6.5\,\%$ of the response at the most sensitive position. Also, non-ideal DFB structures that incorporate grating chirp or other non-uniformities, seem to have sensitivity distributions that are very similar to the actual intensity distributions.

Laser Number	Total length L (mm)	Assymmetry ΔL (mm)	Longit. mode order	Ratio P_{left}/P_{right}	Measured κ (m^{-1})	Wavelength (nm)	Fig.
1	40	0	0	1:1	230	1549	4
2	40	10	0	600:1	230	1549	4
3	50	0	0	–	230	1549	5
3 modified	45 ± 1^a	5 ± 1^a	0	33:1	230	1549	–
4	60	0	-1	–	$-^b$	1533	6

Table 2.1. Overview of the Lasers Characterized in this Paper.
[a]The stated L and ΔL do not take into account possible annealing near the right-hand grating end during fusion splicing.
[b]The value of κ here is expected to be similar to the other lasers because the same UV-exposure level was used.

2.3 Experiments

2.3.1 Setup

The index perturbation sensitivities of four fiber DFB lasers, operating in the 1550-nm band and pumped at 1480 nm, were investigated using the setup shown in Fig. 2.3. An overview of the lasers is given in Table 2.1. Heat from a halogen lamp was focused onto a short length $\delta z = 1$–2 mm of the laser. Length δz determines the spatial resolution of the measurement. The bare fiber had been coated by black ink to improve the heat absorption. A fiber with an Er^{3+}–Yb^{3+}-doped core and a B–Ge-doped photosensitive ring outside the core [19] was used for the lasers.

To minimize effects of ambient temperature fluctuations, we placed the laser close to an aluminium surface. We monitored the lasing frequency by passing the laser output through a scanning Fabry-Perot cavity with a spectral resolution of 1.2 MHz and onto a detector. As the heating position was moved along the fiber, the heat was turned on and off with a shutter, and the resulting frequency shift was recorded.

The exact magnitude of the heat-induced round-trip phase-shift $\delta\phi$ could not be measured directly. $\delta\phi$ can, however, be determined from the measured distribution of $\delta\nu$, for instance by integration of both sides of Eq. (2.5) which thus eliminates the intensity from the expression.

The smallest frequency that could be resolved in the experiment was of the order of 10–30 MHz, limited by random fluctuations in the laser frequency, probably as a result of fluctuations in the ambient temperature and the pump power. Nonuniformities in the black ink coating or in the thermal contact be-

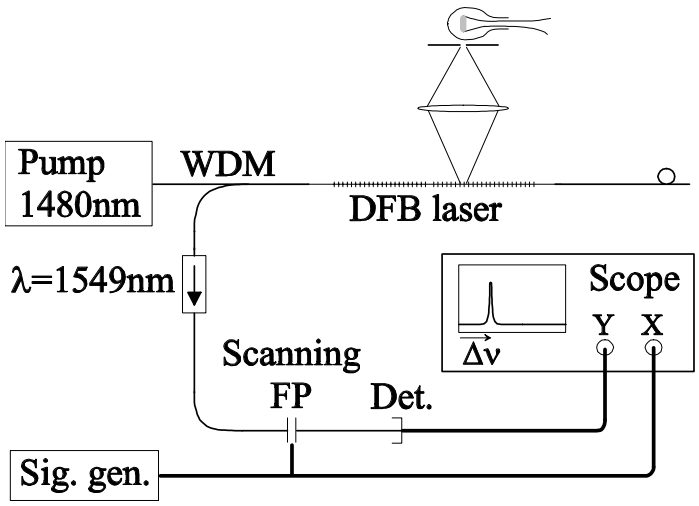

Figure 2.3. Setup for characterizing the phase perturbation sensitivity distribution: WDM, Wavelength division multiplexer; FP, Fabry-Perot interferometer; Det., detector; Sig. gen., signal generator.

tween the fiber and the aluminium may have caused some z dependence of $\delta\phi$.

2.3.2 Symmetric and Asymmetric Lasers

Figure 2.4 shows the measured heat perturbation responses, indicated as squares and circles, for the symmetric laser #1 and the asymmetric laser #2. Both devices lased in two polarizations at wavelengths close to 1549 nm. To within the measurement accuracy, no difference could be observed between the heat-induced perturbation responses of the two polarization modes.

In laser #2, the permanent grating phase-shift was offset by -5 mm from the center, giving a length difference $\Delta L = 10$ mm between the right and left sub-gratings. The corresponding shift in the peak response for that grating is clearly seen from the measurements.

Since the gratings were produced with equal UV-exposures, equal grating strengths are expected. That the grating strengths are equal is confirmed by the measured responses, which both decay exponentially from the phase-shift positions with decay rates corresponding to an effective grating strength of $\kappa = 230\ \mathrm{m}^{-1} \pm 10\,\%$. Calculated heating responses, assuming $\kappa = 230\ \mathrm{m}^{-1}$ and $\delta\phi = 0.53$ rad, are shown as curves in Fig. 2.4. From the UV spot-size used for the grating production, the extension of the permanently phase-shifted region is estimated to be less than 100 μm, which is much less than the $\delta z \approx 2$ mm spatial resolution of the measurements.

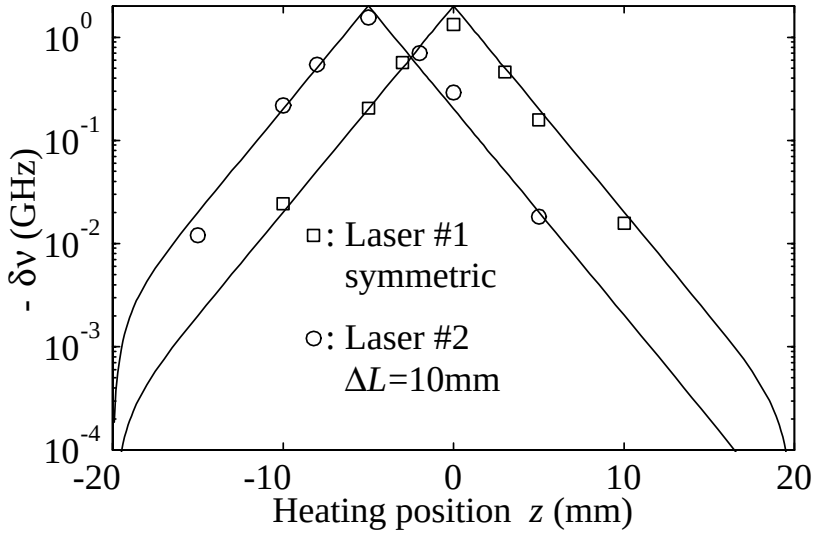

Figure 2.4. Laser frequency responses to heat scans measured for the symmetric laser #1 (squares) and asymmetric laser #2 (circles), both with 40-mm gratings. The lines show calculated responses for $\delta\phi$ =0.53 rad and κ =230 m^{-1}.

When a pump power of 83 mW at 1480 nm was launched into the lasers, the total left + right output powers were 470 μW from laser #1 and 30 μW from laser #2, corrected for losses in the wavelength-division multiplexer and the isolator. The left to right output power ratios were 1:1 for laser #1 and 600:1 ($\pm$10 %) for laser #2. The latter ratio is 6 times higher than predicted by expression (2.4), corresponding to a $\kappa\Delta L$ product that is 39 % higher than expected. The reason for this discrepancy is not clear, but it may be related to grating imperfections that cause nonideal intensity distributions in the regions near the grating ends. In these regions $\delta\nu$ was too small to be resolved by the measurements. Contributions to the power ratios from amplification outside the gratings should be ineligible, as the Er–Yb-fiber was spliced with good quality splices to standard telecom fiber less than 10 mm from the grating ends. The low power efficiency from the asymmetric device can be attributed to the short length and low reflectivity of the left-hand sub-grating [11], causing a higher threshold and reduced slope efficiency.

We obtained a better agreement with theory by cutting the symmetric 50 mm laser #3 (described in the next Subsection 2.3.3) 5$\pm$1 mm from its left end and fusion-splicing it back onto a standard telecom fiber. A total output power of 450 μW at 83-mW pump was obtained with a left-to-right output power ratio of 33. Assuming $\kappa = 230$ m^{-1}, this corresponds to an effective ΔL of 7.6

mm. The 2.6±1 mm increase in ΔL compared to what was cut off is probably due to excessive heating near the left-hand grating end during fusion splicing, annealing out the index modulation.

2.3.3 Polarization-Dependent Grating Strength

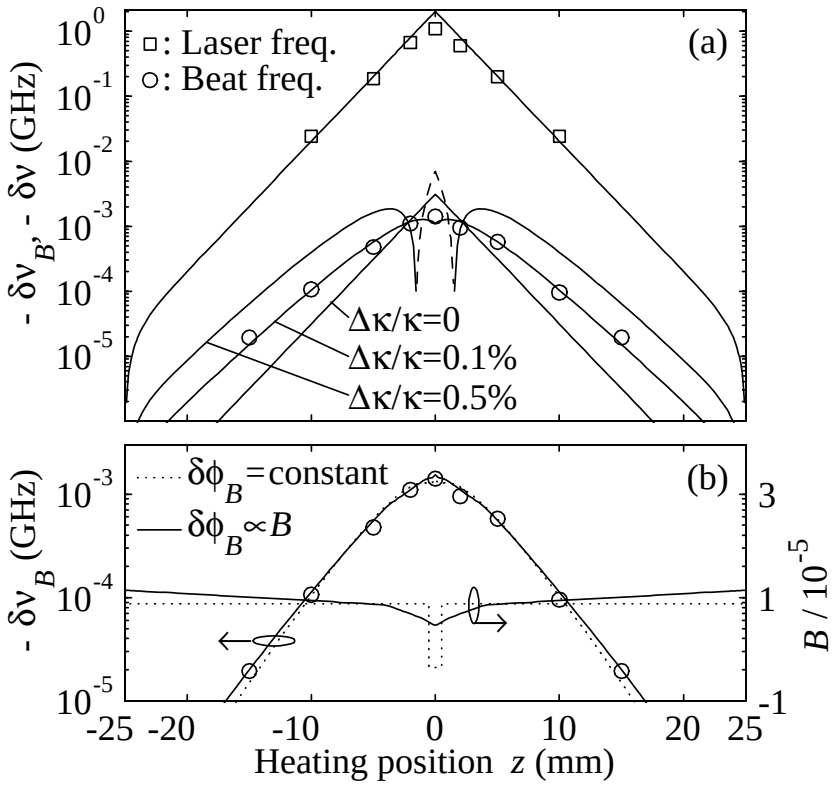

Figure 2.5. (a) Laser frequency and polarization beat frequency responses to heat scan measured for the dual polarization 50-mm DFB laser #3. Upper curve, the calculated laser frequency response $\delta\nu$. The other curves show calculated beat frequency responses $\delta\nu_B$ for three values $\Delta\kappa/\kappa$, assuming z-independence of B. Dashed curve indicates $-\delta\nu_B < 0$. (b) Measured (circles) and calculated (lines) beat frequency responses $\delta\nu_B$ for two different distributions of $B(z)$ when $\Delta\kappa = 0$. For all calculations in both (a) and (b) $\delta\phi$ =0.53rad and κ =230m^{-1} was assumed.

The squares in Fig. 2.5 (a) shows the measured response $\delta\nu$ of the laser frequency to a heat perturbation along symmetric 50-mm laser #3. This laser also operated in two polarizations operating at 1549 nm and produced under practically identical conditions to lasers #1 and #2. Again, the measured re-

sponse fits the calculated response well when $\kappa = 230$ m^{-1} and $\delta\phi = 0.53$ rad are assumed.

By replacing the Fabry-Perot interferometer in Fig. 2.3 with a polarizer and monitoring the detected signal on an rf spectrum analyzer, we measured the polarization beat frequency of laser #3 to be $\nu_B = 971$ MHz, corresponding to a birefringence of $B = n_y - n_x = 7.11 \cdot 10^{-6}$. The heat perturbation response $\delta\nu_B$ of the beat frequency was also measured and is plotted as circles in Fig. 2.5 (a).

Two contributions to $\delta\nu_B$ can be identified. The first contribution comes from the polarization dependence $\delta\phi_B$ of the heat-induced round-trip phase perturbation and should be proportional to $\delta\nu$. The second contribution arises from differences in the spatial distributions of the index perturbation sensitivities of the two modes, which corresponds to different shapes of the modal intensity distributions. This difference may either be due to a polarization dependence $\Delta\kappa$ of the grating coupling coefficient or to polarization dependent grating phase nonuniformities. Such phase nonuniformities are equivalent to a z dependence of the fiber birefringence B. Because the measured $\delta\nu$ and $\delta\nu_B$ are not proportional [*c.f.* Fig. 2.5 (a)], it seems clear that the difference in sensitivity distributions is significant in determining $\delta\nu_B$ for this laser.

If B is assumed to be z independent, the polarization dependence $\Delta\kappa$ of κ may be deduced from the measurements. The three bottom curves in Fig. 2.5 (a) show the calculated $\delta\nu_B$ for different (z independent) values for $\Delta\kappa/\kappa$. A good fit to the measured data is found for $\Delta\kappa/\kappa = 0.1\%$, corresponding to a Bragg modulation of the birefringence with an amplitude of $\Delta B = \Delta\kappa\lambda/\pi = 1.14 \cdot 10^{-7}$, where $\lambda = 1549$ nm.

Alternatively, if $\Delta\kappa$ is assumed to be zero, the z dependence of B can in principle be deduced from the measurements. One complicating question in this case is, however, to which degree $\delta\phi_B(z)$ will be dependent on $B(z)$. If variations in $B(z)$ arise from variable thermal stresses in the fiber [20], a proportional relation $\delta\phi_B \propto B$ is believed to be realistic. The temperature dependence of other possible contributions to $B(z)$, for example, UV-induced birefringence, is not so well understood, and it cannot be clearly determined whether $\delta\phi_B$ is z dependent.

Figure 2.5 (b) shows two different solutions obtained for $B(z)$, assuming either $\delta\phi_B \propto B$ or $\delta\phi_B =$ constant. A manual curve fitting procedure was used in which we adjusted the shape of $B(z)$ until the calculated curves for $\delta\nu_B$ matched the measured data to within reasonable error margins. For $\delta\phi_B =$ constant a second solution for $B(z)$ exists that is similar to the one shown but mirrored about the line $B = 0.71 \cdot 10^{-5}$. No similar second solution can be found for $\delta\phi_B \propto B$.

For simplicity, it was assumed that only n_x depends linearly on $B(z)$ in the calculations, while n_y was kept constant. This introduces grating phase errors in the x-polarized mode only, leading to a slightly wider spatial distribution of the index perturbation sensitivity for that mode. Practically the same solutions for $B(z)$ is obtained when we assume that both n_x and n_y are z dependent, provided that a small error in the permanent grating phase-shift at $z = 0$ is assumed.

The birefringence non-uniformities shown in Fig. 2.5 (b) are both larger in amplitude and much more localized than expected for the fiber used. UV-induced birefringence fluctuations of such a magnitudes are not likely, as the grating was produced by pulsed UV-laser scanning fiber technique in which the grating phase is directly controlled by the timing of the UV pulses relative to fiber's position as the fiber is scanned through a spot made from interfering UV-beams. This eliminates the need for extra UV-exposure in the phase-shifted region. It may therefore be concluded that the observed variations in $\delta\nu_B/\delta\nu$ most probably is due to a polarization dependence of the grating strength by 0.1 %, illustrated in Fig. 2.5 (a).

Note that the multiple solutions in Fig. 2.5 (b) imply that $\Delta\kappa$ cannot be easily deduced from measurements of $\delta\nu_B$ if $B(z)$ is not known in advance to some accuracy. Methods have been demonstrated for measuring fiber birefringence with potentially high spatial resolution [21] and could be used for this purpose.

UV-induced birefringence in low birefringence Ge-doped fibers ranging up to 8 % of the total index change, depending on the polarization of the UV beam, have been reported [22]. Similar values for $\Delta\kappa/\kappa$ should thus be possible. When we wrote the DFB-gratings characterized in this paper, the UV light was polarized approximately parallel to the fiber axis to minimize UV-induced birefringence. The remaining birefringence modulation ΔB, may be due to a small remaining component of the UV polarization orthogonal to the fiber axis, or to an asymmetric UV exposure of the photo-sensitized ring owing to the large amount of UV absorption in silica.

2.3.4 Higher-Order Mode Operation

The squares in Fig. 2.6 (a) show the measured response $\delta\nu$ of the laser frequency to heat perturbation along symmetric $L = 60$ mm laser #4 operating at 1533 nm. From the UV-exposure used, κ is expected to be 230 m^{-1} also for this laser, giving a rather large κL product of 13.8. It seems clear from the measurements that the laser operates in a higher order mode. We believed that the observed mode is of the first order, since the gain thresholds generally are expected to increase with modal order, *c.f.* Subsection 2.2.1. The relatively small width of the dip in $\delta\nu$ near $z = 0$ also supports this conclusion.

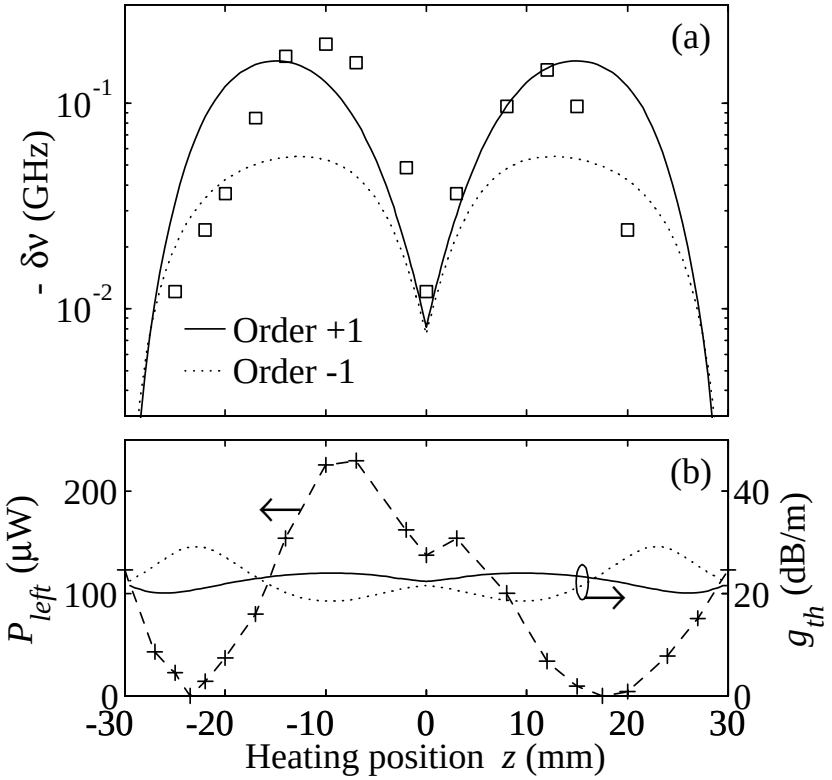

Figure 2.6. (a) Laser frequency response (squares) to heat scan measured for 60-mm DFB laser #4 with similar grating parameters to those characterized in Figures 3 and 4. Calculated responses of the +1- (solid curves) and −1- (dotted curves) order modes with $\delta\phi = 0.2$ rad are also shown. (b) Measured output power from the left end P_{left} (crosses) and calculated threshold gain for the +1 (solid curves) and -1 (dotted curves) order modes plotted versus heating position when $\delta\phi = 0.2$ rad.

The calculated frequency responses of the +1- and −1-order modes to a perturbation of $\delta\phi = 0.2$ rad are also shown in the figure. These responses are not identical, as they would be for much smaller perturbations. This difference is due to the very close frequency spacing of the first and second order modes, leading to a highly non-linear relationship between $\delta\phi$ and $\delta\nu$, *c.f.* requirement 1. in Subsection 2.2.2 [7]. When $\delta\phi$ increased, the calculated maximum value of the −1 mode response saturated towards 0.09 GHz for $\delta\phi \gtrsim 0.7$rad. This is well below the measured maximum of 0.19 GHz, indicating that the characterized mode is of the +1 order.

The left output power from the unperturbed laser was $P_{left} = 120\,\mu$W, corrected for losses in the wavelength-division multiplexer and isolator. However, P_{left} was found to be strongly affected by the position of the heat-perturbation, as can be seen from Fig. 2.6 (b) (crosses). At the heating positions $z = -23.5$ mm and +17.5 mm the laser is brought just below threshold while the power increases by 85 % compared to the unperturbed situation at $z = -8$ mm. This variation in output power with heating position may explain the discrepancy between theory and experiment in Fig. 2.6 (a), as the laser frequency is expected to decrease with increasing lasing power due to heating of the cavity from non-radiative losses at the lasing wavelength and conversion between pump and laser photon energies. The deviations between the measurements and the simulated +1-mode response in Fig. 2.6 (a) correlates well with the observed variations in output power. When we varied the lasing power by changing the pump power, a frequency shift of 0.87 MHz per μW of output power could be observed. Some of this shift may be due to non-radiative losses at the pump wavelength. The discrepancy from theory seen in Fig. 2.6 (a) corresponds to a shift of 0.4–0.6 MHz/μW.

The fundamental mode would also be expected to lase in this device, because the gain threshold for this mode should normally be much lower than for the higher-order modes. However, the fundamental mode could not be observed with the Fabry Perot interferometer, possibly partly because of asymmetric grating imperfections that could have caused most of the fundamental mode output power to exit at the right-hand end, which was not monitored in the experiment. The asymmetric shape of the measured response in Fig. 2.6 (a) supports this explanation. Competition with the higher order mode may also play a role in reducing the fundamental mode lasing power. Further, any losses within the cavity would reduce the slope efficiency much more for the fundamental mode than for the higher order mode because of the high cold-cavity Q factor of the fundamental mode.

The calculated threshold gain versus heating position for the +1 and −1 order modes are also shown in Fig. 2.6 (b). Again there is a qualitative agreement between the calculated +1-order mode threshold and the measured output

power. The maximum gain of the fiber used, measured before UV-exposure and with 1480 nm pumping, was 15.2±1 dB/m at the laser wavelength. This is below the calculated and plotted threshold gains, which are in the range from 18 to 30 dB/m. Distributed grating phase errors may, however, bring the +1 order mode threshold down below 15 dB/m without changing the qualitative shape of the perturbation response. Such phase errors could arise from self heating owing to circulating high intensities in the fundamental mode near $z = 0$.

2.4 Conclusion

A heat-scan technique for characterization of DFB lasers has been demonstrated experimentally and investigated numerically and through comparison with an existing perturbation theory for electromagnetic resonators [7, 8]. Both the theory and the obtained numerical results indicate that the perturbation sensitivity will to a large extent be proportional to the modal intensity distribution.

Grating properties such as the coupling parameter κ, the polarization dependence $\Delta\kappa$ of κ, and the position of the grating phase-shift can be deduced from the measured heating sensitivity distributions ν and ν_B. Because the perturbation sensitivity depends on both the κ distribution and the grating phase distribution, one generally needs to know none one of these distributions is in general required to determine the other. For instance, to deduce $\kappa(z)$ from the measured $\Delta\nu(z)$ in Figs. 2.4 and 2.5, we had to assume a perfect grating phase. There is a similar relation between the abilities to determine $\Delta\kappa(z)$ or $B(z)$ from $\Delta\nu_B(z)$, as illustrated by the different beat-frequency simulations in Fig. 2.5 (a) and (b).

Without *a priori* knowledge of any of the grating parameters, the method still reveals the shape of the modal intensity distributions with good accuracy. This information is directly related to important topics such as the cold cavity Q factor, gain thresholds, pump efficiencies and non-linear effects such as gain hole burning, gain-dependent refractive-index changes and Kerr nonlinearities.

The experimental setup described in this paper is relatively simple, and easy to implement. Significant improvement in accuracy is however expected with a more refined setup. Better temperature stabilization of the laser, for instance by immersion of the laser into a liquid with a high specific heat capacity, would reduce both the random frequency noise and the systematic errors related to self-heating of the laser discussed in Subsection 2.3.4.

If the heat perturbation technique is to be used to characterize semiconductor DFB lasers, a much more localized heating spot would be required, because of the much smaller dimensions of the devices. This type of heating spot could

be achieved by use of a focused laser beam for the heating. A relatively high heat-modulation frequency would probably be required to avoid broadening of the heated region by thermal diffusion.

An important application of the heat perturbation method is characterization of the spatial sensitivity distribution of fiber laser sensors with laser frequency readout, polarization beat frequency readout, or both [23]. Theoretically, the sensitivity of such DFB-lasers will decay from the center position proportionally to $\exp(-2\kappa|z|)$, giving an effective sensitive length of κ^{-1}. The sensitivity distribution of polarimetric sensors may, however, deviate significantly from the ideal case in the presence of a moderate polarization dependence of the grating strength or with non-uniform birefringence distributions, as illustrated by the simulated curves in Fig. 2.5.

2.5 Acknowledgment

This study was sponsored by Optoplan AS, the Norwegian Research Council and British Council. The Optoelectronics Research Center is an interdisciplinary research center funded by the Engineering and Physical Sciences Research Council, UK.

References

[1] L. J. P. Ketelsen, I. Hoshino, and D. A. Ackerman, "The Role of Axially Nonuniform Carrier Density in Altering the TE-TE Gain Margin in InGaAsP-InP DFB Lasers", IEEE J. Quantum Electron. **27**, 957–964 (1991).

[2] M. R. Phillips, T. E. Darchie, and E. J. Flynn, "Experimental Measure of Dynamic Spatial-Hole Burning in DFB lasers", IEEE Photonics Technol. Lett. **4**, 1201–*120*3 (1992).

[3] W. H. Loh, B. N. Samson and J. P. de Sandro, "Intensity profile in a distributed feedback fibre laser characterized by a green fluorescence scanning technique", Appl. Phys. Lett. **69**, 3773–*3775* (1996).

[4] W. Margulis, I. C. S. Carvalho, P. M. P. Gouvêa, and B. Lesche, "Heat scan: a simple technique to characterize gratings in fibers", Opt. Lett. **18**, pp. 1016–*1018*, 1993.

[5] S. Sandgren, B. Sahlgren, A. Asseh, W. Margulis, F. Laurell, R. Stubbe, and A. Lidgard, "Characterization of Bragg gratings in fibers using the heat-scan technique", Electron. Lett. **31**, pp. 665–*666*, 1995.

[6] E. Brinkmeyer, G. Stolze, and D. Johlen, "Optical space domain reflectometry (OSDR). for determination of strength and chirp distribution along optical fiber gratings" in *Bragg Gratings, Photosensitivity and Poling in Glass Fibers and Waveguides*, Vol. 17 of 1997 OSA Technical Digest Series, (Optical Society of America, Washington D.C., 1997).

[7] A. Cunliffe and L. E. S. Mathias, "Some perturbation effects in cavity resonators", Proc. Inst. Electron. Eng. **97**, 367–376 (1950).

[8] H. B. G. Casimir, "On the theory of electromagnetic waves in resonant cavities", Phillips Res. Rep. **6**, 162–182 (1951).

[9] E. Rønnekleiv, M. Ibsen, M. N. Zervas and R. I. Laming, "Characterization of intensity distribution in symmetric and asymmetric fiber DFB lasers", in *Conference on Lasers and Electro-Optics*, Vol. 6, of 1998 OSA Technical Digest Series, (Optical Society of America, Washington D.C., 1997).

[10] J. T. Kringlebotn, J. L. Archambault, L. Reekie, and D. N. Payne, "Er^{3+}:Yb^{3+}-codoped fiber distributed-feedback laser", Opt. Lett., **19**, 2101–2103 (1994).

[11] V. C. Lauridsen, T. Søndergaard, P. Varming, and J. H. Povlsen, "Design of Distributed Feedback Fibre Lasers" in *Proceedings of the European Conference on Optical Communications '97*, (institution of Electrical Engineers, London, 1997) Vol. 3, pp. 39–42.

[12] H. Soda, Y. Kotaki, H. Sudo, H. Ishikava, S. Yamakoshi, and H. Imai, "Stability in Single Longitudinal Mode Operation in GaInAsP/InP Phase-Adjusted DFB Lasers", IEEE J. Quantum Electron. **QE-23**, 804–814 (1987).

[13] E. Rønnekleiv and O. Hadeler, "Stability of an Er-Yb-doped fiber distributed-feedback laser with external reflections", Opt. Lett. **24**, 617–619 (1999).

[14] G. A. Ball, C. G. Hull-Allen and J. Livas, "Frequency Noise of a Bragg grating fibre laser", Electron. Lett. **30**, 1229–1230 (1994).

[15] G. Björk and O. Nilsson, "A New Exact and Efficient Numerical Matrix Theory of Complicated Laser Structures: Properties of Asymmetric Phase-Shifted DFB Lasers", *J. Lightwave Technol.*, **LT-5**, pp. 140-146 (1987).

[16] M. Yamada and K. Sakuda, "Analysis of almost-periodic feedback slab waveguides via a fundamental matrix-approach", *Appl. Opt.*, **26**, pp. 3474-3478 (1987).

[17] G. P. Agrawal, A. H. Robeck, "Modeling of Distributed Feedback Semiconductor Lasers with Axially-Varying Parameters", *IEEE J. Quantum Electron.*, **24**, pp. 2407-2414 (1988).

[18] E. Rønnekleiv, M. N. Zervas and J. T. Kringlebotn, "Modelling of Polarization Mode Competition in Fiber DFB Lasers", IEEE J. Quantum Electron. **34**, 1559–*1569* (1998).

[19] L. Dong, W. H. Loh, J. E. Caplen, J. D. Minelly and L. Reekie, "Efficient single-frequency fiber-lasers with novel photosensitive Er/Yb optical fibers", Opt. Lett. **22**, 694–*696* (1997).

[20] J. I. Sakai and T. Kimura, "Birefringence Caused by Thermal Stress in Elliptically Deformed Core Optical Fibers", IEEE J. Quantum Electron. **QE-18**, 1899–1909 (1982).

[21] A. Simon and R. Ulrich, "Evolution of polarization along a single-mode fiber", Appl. Phys. Lett. **31**, 517–521 (1977).

[22] T. Erdogan and V. Mizrahi, "Characterization of UV-induced birefringence in photosensitive Ge-doped silica optical fibers", J. Opt. Soc. Am. B **10**, 2100–*2105* (1994).

[23] O. Hadeler, E. Rønnekleiv, M. Ibsen and R. I. Laming, "Polarimetric fiber distributed feedback laser sensor for simultaneous strain and temperature measurements", Appl. Opt. **38**, 1953–1959 (1999).